

DETC2015-46228

## RACK FORCE ESTIMATION FOR ELECTRIC POWER STEERING

**Thomas Weiskircher \***

Applied Dynamics & Control  
Research Group, International  
Center for Automotive Research,  
Clemson University,  
Greenville, South Carolina, 29607  
Email: tweiski@g.clemson.edu

**Steve Fankem**

Institute for Mechatronics in  
Mechanical and Automotive  
Engineering, TU Kaiserslautern,  
67663 Kaiserslautern, Germany  
Email: steve.fankem@mv.uni-kl.de

**Beshah Ayalew**

Applied Dynamics & Control  
Research Group, International  
Center for Automotive Research,  
Clemson University,  
Greenville, South Carolina, 29607  
Email: beshah@clemson.edu

### ABSTRACT

*This paper discusses a steering rack force estimation scheme using test-rig generated models. In addition to friction identification, a model of the electric power steering system is identified by the use of the instrumented test-rig. It turns out that the friction in the steering system is highly load-dependent, asymmetric with respect to speed, and shows no Stribeck effects. A LuGre model is adopted and fitted to approximate the measured dynamic friction. Consequently, this model is used in a friction compensator which is combined with a linear disturbance observer to estimate the steering rack force. The proposed estimation scheme is analyzed via evaluated system simulations and experiments on the steering system test-rig. Finally, considering the fact that the friction level varies with each steering device manufactured and installed, the paper discusses algorithms for friction level adaptation.*

### INTRODUCTION

In the recent years, the automotive industry is substituting hydraulic steering systems by their electrical counterparts for higher fuel efficiency and weight savings. Electric power steering (EPS) systems offer the possibility of refining the steering feel via elaborated control methods that exploit their simplicity and speed of response. Furthermore, various driver assistance functions such as lane departure warning and lane keeping as-

ist are more readily enabled with EPS. For many EPS functions, the steering rack force generated by the tire ground forces (contributing to the total tire aligning moment) plays an important role: e.g. steering feel is directly related to the steering torque transferred to the steering wheel [1,2]. Some advanced functions such as the estimation of the tire lateral friction coefficient can be improved by additional information about the total tire aligning torque/rack force, see [3,4]. Since available sensors are often limited to the column torque sensor (also known as torsion bar) and the EPS motor torque and speed sensors, on-line rack force estimation schemes are required to enable these functions. However, since this estimation schemes are highly influenced by the friction in the EPS, a friction compensation scheme is required, especially when the rack force is at low levels.

Another idea for the estimation of the steering rack force includes the incorporation of the vehicle dynamics sensors and a high fidelity model of the vehicle dynamics (e.g. including suspension, tire models, and further components) [4,5]. It turns out that the quality of the estimated rack force highly depends on the model parameters and sensors included and thus, is not sufficiently exact in some driving situations. An additional application of the rack force is found in the area of driving simulators with human in the loop [6]. Here, an approach to enhance the realism and fidelity of the steering feel with the estimated rack force is proposed. In contrast to the present contributions, no torsion bar sensor is available and the estimation of the driver steering wheel torque is necessary. The friction includes only a

---

\*Address all correspondence to this author.

damping part and no Stribeck or dry friction characteristics, and thus, the steering dynamics model is of linear type.

In our previous research [7], a detailed steering system dynamics model was introduced and the basic idea of the rack force estimation was outlined. It turns out that the estimation of the rack force is possible with a linear disturbance observer combined with feed-forward friction compensation. However, the static Stribeck friction model used there gave insufficient results with sign changes in the steering speed and in the low speed range. Furthermore, the assumption of load-independent friction was a gross simplification since experiments indicate that the friction is indeed load-dependent. Therefore, in this paper to address these deficiencies, we adopt the LuGre dynamic friction model and identify its parameters using test-rig generated data. The model of the EPS from the previous research is combined with the new friction model and used for algorithm design and evaluation. The estimation algorithm is analyzed by means of the simulation model first, and compared with the test-rig measurements. We close the contribution by discussing two algorithms for friction level adaptation to take into account varying friction levels with each steering device manufactured and installed, even on otherwise identical vehicles.

## SYSTEM MODELING

### Electric Power Steering System Overview

In EPS several types of system layouts are common, e.g. rack-assisted EPS, active-EPS, pinion-assisted EPS etc. In all layouts, electric motors are connected to the steering mechanics to influence the dynamic and static behavior. An ECU with a control algorithm reads sensor information from a steering wheel speed/position sensors, a motor speed sensor and a torsion bar sensor and acts to control the motor. In the system we analyze, which is depicted in Fig. 1, the torque sensor installed in the steering column measures the torque between the pinion and the steering wheel. This gives us an idea of the torque input applied by the driver to the steering wheel/system to solicit the lateral response from the vehicle. From the other end of the steering system, the total tire aligning torque (of all ground forces and moments governing the vehicle dynamics), the inertia and the friction between the mechanical parts of the steering and suspension system act against this driver input. To keep the necessary driver input to overcome this reaction on a comfortable level and generate a desired steering feel, the electric motor assists the driver by compensating for this reaction up to a certain level.

### EPS Dynamics Model

Here we briefly first introduce a mathematical model of the steering system dynamics. The high fidelity system from Fig. 1 is reduced to five lumped masses, see Fig. 2. Table 1 gives the list of the parameters and symbols used herein. To reduce the num-

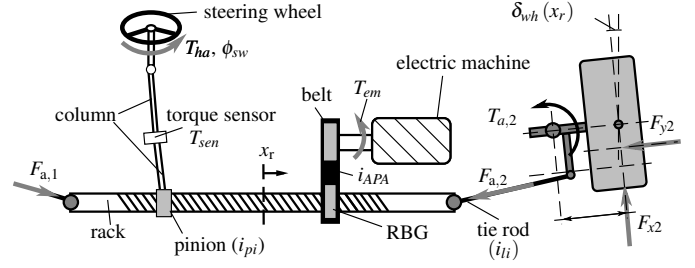


FIGURE 1. RACK-TYPE EPS LAYOUT

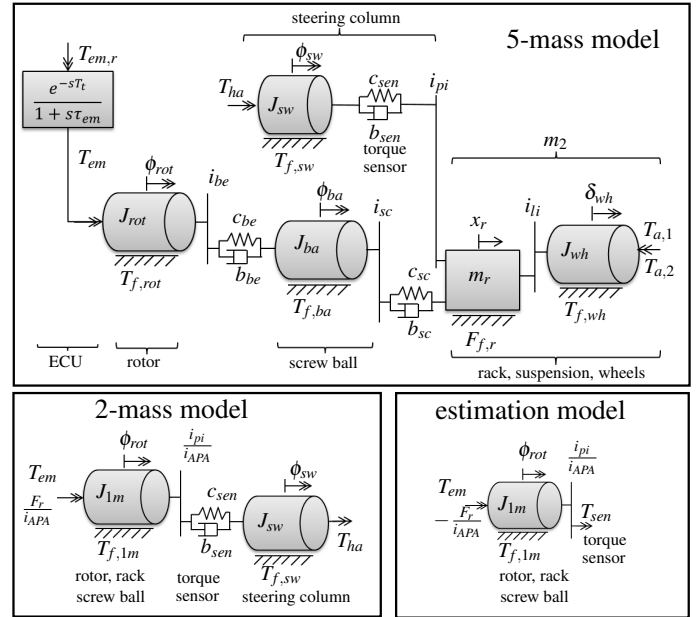


FIGURE 2. REDUCTION OF THE LUMPED 5-MASS STEERING SYSTEM MODEL FOR RACK FORCE ESTIMATION

ber of required parameters to be identified beforehand as well as the computational burden of the on-line estimator, the system model can be reduced step-by-step to a simplified 2-mass model that works for the relevant frequency ranges for the present application ( $\leq 10$  Hz) [7]. To this end, the connection between the electric motor and rack, which is assumed to be of high stiffness, is reduced to the ratio  $i_{APA}$ . The only required parameters are then the steering column inertia, the resulting inertia on the rack side, and the sensor stiffness and damping, which are given by the sensor specifications. This system has three inputs, namely the driver hand wheel torque  $T_{ha}$ , the steering rack force  $F_r$  and the added electric motor torque  $T_{em}$ . So, even with this 2-mass model, it is not possible to isolate the exact rack force. To overcome this difficulty, the steering column torque sensor can be used to further reduce the model to a 1-mass model. Here,

the measured input  $T_{sen}$  substitutes the steering column dynamics and driver/motor inputs, and only the lumped effective inertia of the steering rack with screw ball gear and motor remains. As the steering motor torque is estimated within the ECU, one may think of estimating the value of  $F_r$  with a simple force-torque balance equation. In fact, this leads to inaccurate results because of the friction in the system.

The dynamics of the 1-mass model depicted in Fig. 2 is given by:

$$T_{1m} = T_{em} + (i_{pi}/i_{APA})T_{sen}, \quad (1a)$$

$$J_{1m} = m_r/i_{APA}^2 + (i_{ti}/i_{APA})^2 J_{wh} + J_{rot} + (1/i_{be})^2 J_{ba}, \quad (1b)$$

$$\dot{\phi}_{rot} = \omega_{rot}, \quad (1c)$$

$$J_{1m}\dot{\omega}_{rot} = T_{1m} - F_r/i_{APA} - T_{f,1m}, \quad (1d)$$

with the joint control input  $T_{1m}$  and the resulting inertia  $J_{1m}$ . As indicated by the system state variable  $\phi_{rot}$  the system is formulated on the motor side of the ball gear drive. The rack force is generated by the tie rod forces  $F_r = F_{a,1} + F_{a,2}$ . In fact, the non-linearity of the system Eqn. (1) results only from the nonlinear friction  $T_{f,1m}$ , which will be detailed in the following section.

The remaining assumptions of the simplified model are: the effective inertia  $J_{1m}$  is known and that there is little backlash in the ball gear drive and the pinion. Note that the friction force and the rack force are two unknown inputs; the estimation task still has to isolate the rack force. All ratios are assumed to be constant in the main operation range of the steering system.

## Friction Model

Friction modeling and compensation have a long history mainly in position control of different types of machines actuated with electric drives. The main effects observed in friction related research are dry friction caused by interaction of rough surfaces, viscous friction of surfaces with lubricants between them, and hysteresis [8, 9]. As far as models for friction, the Dahl and the LuGre models [10, 11] are broadly applied in friction compensation in precise machine position control [12–17]. Most of these works focus on machines for pure positioning with no load or a known load.

The case of vehicle steering systems differs from this in two ways: First, no position control is used in conventional steering systems, and therefore, no control error information is available for the friction identification process [18, 19]; Second, the external load (tire-ground reaction) is unknown, as is the friction in the system. Therefore, their separation is a non-trivial task. Still, some model-based compensation could be attempted to estimate and account for friction in the steering system. In our previous work, we found that using simple static Stribeck-like friction models (with speed-dependent static, dry friction and viscous terms) are only useful for a rough estimation and compensation

**TABLE 1.** EPS PARAMETERS AND SYMBOLS

Name	Symbol	Unit
motor delay time	$T_l$	s
motor time constant	$\tau_{em}$	s
rotor inertia	$J_{rot}$	kgm <sup>2</sup>
steering wheel inertia	$J_{sw}$	kgm <sup>2</sup>
ball screw inertia	$J_{ba}$	kgm <sup>2</sup>
wheel inertia	$J_{wh}$	kgm <sup>2</sup>
rack mass	$m_r$	kg
rack mass with road wheels	$m_2$	kg
belt stiffness	$c_{be}$	Nm/rad
belt damping	$b_{be}$	Nms/rad
ball gear stiffness	$c_{sc}$	N/m
ball gear damping	$b_{sc}$	Ns/m
torsion bar sensor stiffness	$c_{sen}$	Nm/rad
torsion bar sensor damping	$b_{sen}$	Nms/rad
belt ratio	$i_{be}$	-
ball gear ratio	$i_{sc}$	rad/m
tie rod ratio	$i_{ti}$	rad/m
pinion ratio	$i_{pi}$	rad/m
rack to rotor ratio	$i_{APA}$	rad/m

of the friction. In the present paper, we adopt the dynamic LuGre friction model [10, 11]. The model equations are:

$$\dot{z} = \omega_{rot} - \frac{|\omega_{rot}|}{T_{fs}} \sigma_0 z, \quad (2a)$$

$$T_{fs} = T_c + (T_s - T_c) \exp - (\omega_{rot} / \omega_{rot,s})^2, \quad (2b)$$

$$\sigma_1 = \sigma_{1,0} \exp - (\omega_{rot} / \omega_{rot,\sigma_1})^2, \quad (2c)$$

$$T_f = \sigma_0 z + \sigma_1 \dot{z} + \sigma_2 \omega_{rot}. \quad (2d)$$

$z$  is the state of the system representing deflection of some virtual, microscopic bristles, while  $\omega_{rot}$  is the input.  $\sigma_0$  and  $\sigma_1$  are the stiffness and damping parameters of the bristles in the contact surface, and  $T_{fs}$  is a general speed-dependent nonlinear static friction function map with static level  $T_s$  and dry (Coulomb) friction level  $T_c$ . Then,  $\omega_{rot,s}$  marks the local minimum of this nonlinear friction for values  $|\omega_{rot}| > 0$ .

Furthermore, from the nature of friction, it is known that the load between the mechanical parts plays an important role. A modification of the LuGre model is needed to include this effect via a load-dependent map as will be detailed in the next section.

## DESCRIPTION OF TEST-RIG AND IDENTIFICATION

### Steering Test-Rig

The steering test-rig is shown in Fig. 3 and a detailed description is given in [20]. The main functionality of the test-rig used here is the excitation of the system with an electric linear motor connected to a tie rod and the measurements including rack force, rack position, steering wheel speed and position. Also, the series-production steering system tested has an open ECU-software which allows reading and overriding the torque output of the steering motor commanded by a dSpace real-time prototyping system via a CAN bus.

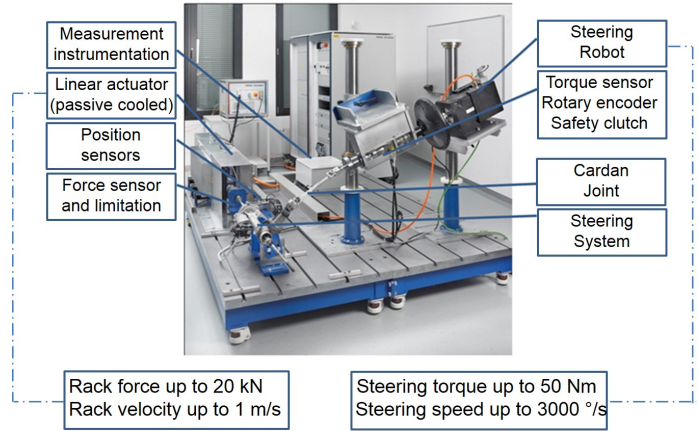


FIGURE 3. DESCRIPTION OF STEERING TEST-RIG

### Measurement and Identification of Friction Model

As the main mechanical and electrical specification of the steering system are known (e.g. inertia, gear ratios, torsion bar sensor stiffness), only the friction parameters are left for identification. In contrast to the computationally intensive techniques proposed in [21–25] which use minimum least squares and special excitations, the static friction level was identified in this work using constant speed profiles controlled by the steering robot motor. Several repetitions were done for each speed setting. The more important part is the pre-load of the steering system (as known rack force) by the linear motor for each speed selected. To prevent the steering system from running into its mechanical stop, the EPS motor compensates for this pre-load. Assuming exact pre-load compensation, the steering robot only controls the rack speed at constant value which simplifies the controller settings for the steering robot machine. The pre-load is measured with a high-quality force sensor mounted between linear motor and tie road. The torque sensor is used to measure the friction force in this setting. The static friction maps obtained are shown in Fig. 4. The measurement was done in two speed quadrants, and a range of rack force upto 3000 N.

As expected, the friction varies almost linearly with pre-load, while the speed has no clear influence. This means that the viscous damping is nearly zero. The friction level is asymmetric with direction or sign of speed and there are no clear Stribeck effects. Only for very small load values is a Stribeck effect seen, but with a very small rise over the dry friction level. Thus, for further analysis, the Stribeck effect is neglected. The static friction map is then connected to the dynamic LuGre friction model and the static friction value is selected by speed and load and fed to the model. Since the viscous damping is negligible, the value of the parameter  $\sigma_2$  is set to zero. Thus, only the parameters  $\sigma_0, \sigma_{1,0}$  remain to be identified. Note that with the steering sys-

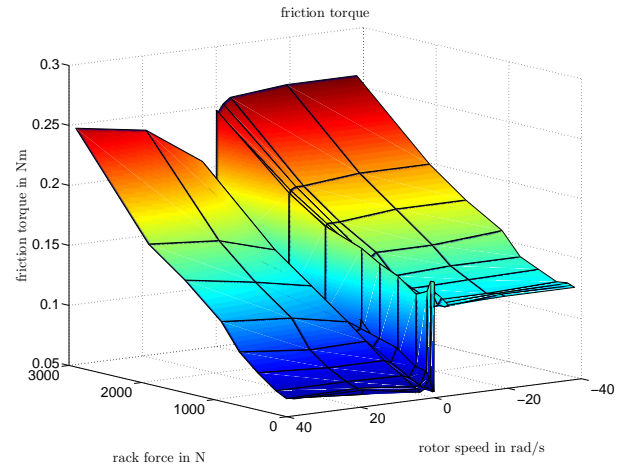
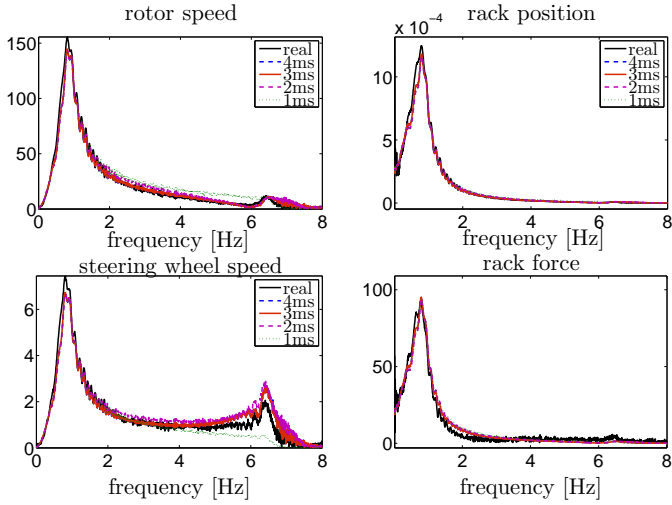


FIGURE 4. EPS FRICTION MEASURED IN TWO QUADRANTS USING TEST-RIG

tem model reductions adopted, this identification of the dynamic LuGre friction model parameters gives only virtual parameterization of the friction level in the steering system with the test rig. The friction estimation results are detailed in the main results section.

### Validation of Steering System Models

The test rig is also used for validation of the models for the EPS. Fig. 5 shows frequency domain responses of the different orders of the EPS model. The results are generated by the test-procedure in Fig. 6. Herein, the excitation is generated by the steering motor while the linear motor generates a spring-damper force to prevent the steering rack of running into its mechanical stops. The result shows good approximation of the real system in the frequency range of interest for all models. It should be



**FIGURE 5.** VALIDATION OF THE EPS MODELS USING A TEST-RIG AND SINE SWEEP INPUT ( $T_{em,r} = 0..4$  Nm from 0 Hz - 8 Hz) - FREQUENCY DOMAIN

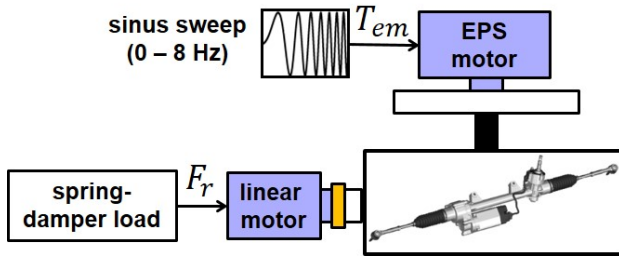


**FIGURE 6.** DESCRIPTION OF TEST PROCEDURE USING STEERING TEST-RIG

noted that the 1-mass (1ms) model in this figure is not exactly the model conceptualized in Eqn. (1) with the torque sensor signal as its additional input. Instead, it is a fully condensed model with all masses in the steering system. Moreover, the 2-mass (2ms) model in the frequency analysis is the model depicted in Fig. 2 on the lower left side.

### Reductions of Static Friction Model

As the rack force estimation that will use the friction models needs to be executable on a real series production ECU, further simplifications of the friction models are required. Therefore, the complex two-dimensional (speed, load) friction map is approximated by:

$$\hat{T}_{fs}(\omega_{rot}, F_r) = \begin{cases} k_0^+ + k_\omega^+ |\omega_{rot}| + k_r^+ |F_r| & \text{for } v \geq 0 \\ k_0^- + k_\omega^- |\omega_{rot}| + k_r^- |F_r| & \text{for } v < 0 \end{cases} \quad (3)$$

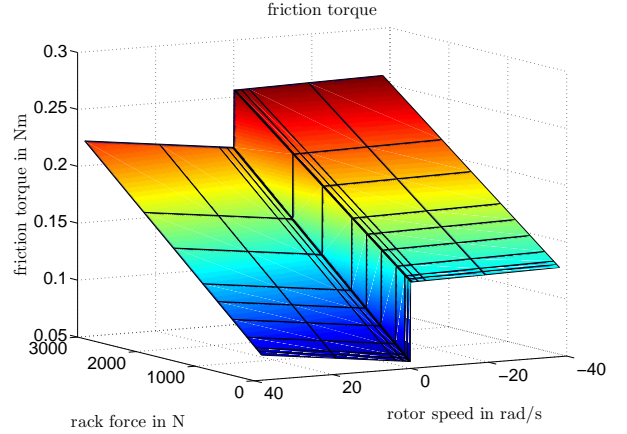


**FIGURE 7.** LINEARIZED STATIC FRICTION MAP WITH RESPECT TO SPEED AND LOAD

Six parameters are required for this linear approximation of the static friction map, three for each speed direction: the offset level  $k_0^\pm$ , the steering system load gain  $k_r^\pm$  and the viscous damping coefficient  $k_\omega^\pm$ . Figure 7 shows the results of the approximation with values given in Tab. 2. It should be noted that the effect of the steering system load (namely, the rack force) is up to one order higher than that of the speed. Furthermore, the parameters in the table show that, with changes in direction (sign of speed), the load has almost a symmetric effect on the friction as opposed to the damping coefficient.

**TABLE 2.** PARAMETERS OF THE FRICTION APPROXIMATION

Parameter	Value	Unit
$k_0^+$	$5.600 \cdot 10^{-2}$	Nm
$k_0^-$	$1.258 \cdot 10^{-1}$	Nm
$k_\omega^+$	$4.195 \cdot 10^{-4}$	Nm/s
$k_\omega^-$	$6.658 \cdot 10^{-5}$	Nm/s
$k_r^+$	$4.993 \cdot 10^{-5}$	Nm/N
$k_r^-$	$4.345 \cdot 10^{-5}$	Nm/N
$\sigma_0$	4.5	Nm
$\sigma_{1,0}$	0.075	Nms
$\omega_{\sigma_1}$	0.75	rad/s

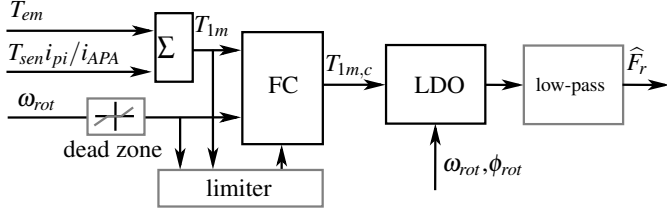


**FIGURE 8.** RACK FORCE ESTIMATION SCHEME WITH LDO AND FC (FC - FRICTION COMPENSATION, LDO - LINEAR DISTURBANCE OBSERVER,  $\hat{F}_R$  - ESTIMATED RACK FORCE)

### RACK FORCE ESTIMATION SCHEME

Figure 8 shows the block diagram for the overall rack force estimation scheme. First, the friction is estimated using the measured speed via the proposed model. Then, the input from the EPS motor and the torque sensor are added to the friction output resulting in a feed-forward friction compensation term. The resulting compensated torque  $T_{1m,c}$  serves as the input to a linear disturbance observer which estimates the final rack force. Each block is discussed in detail in the following subsections.

### Model-based Friction Compensation

The friction compensation module shown in Fig. 8 is introduced to remove the nonlinear friction contribution. It is assumed that the friction is modeled and approximated well ( $\hat{T}_{f,1m} \approx T_{f,1m}$ ) and acts as one of the inputs in eq. (1d). To improve the performance of the compensator under noisy measurements of  $\omega_{rot}$ , other blocks are added: a dead zone element prevents a noisy (drifting) friction compensation at zero speed, while a friction torque limiter reduces the friction when the steering speed is near by zero with the simple algorithm:

$$\begin{aligned} &\text{if } |\omega_{rot}| < SP_A \quad \& \quad |\dot{\omega}_{rot}| < SP_B \\ &\quad T_f = \text{sign}(T_f) \cdot \min(|T_f|, |T_{1m}|) \\ &\text{endif} \end{aligned} \quad (4a)$$

This function incorporates set-points (SP) for the speed and the acceleration to detect standstill conditions of the steering system and to limit the friction. The acceleration signal is calculated by a low-pass filtered numerical derivative of the speed sensor signal. After adding the approximated friction torque to the input of the 1-mass model, the remaining linear system reads

$$J_{1m} \dot{\omega}_{rot} = T_{1m} - F_r / i_{APA} - T_{f,1m} \quad (5a)$$

$$\approx T_{1m,c} - F_r / i_{APA} \quad (5b)$$

Hence, only the friction compensated input torque  $T_{1m,c}$  and the rack force act on the inertia of this reduced 1-mass system.

### Linear Disturbance Observer

For the design of the disturbance observer, the linear system of the 1-mass model is transformed to a linear state-space description:

$$\dot{\mathbf{x}}_s = \mathbf{A}_s \mathbf{x}_s + \mathbf{B}_s u_s + \mathbf{E}_s x_d \quad (6a)$$

$$\mathbf{y}_s = \mathbf{C}_s \mathbf{x}_s. \quad (6b)$$

where:

$$\mathbf{x}_s = \begin{bmatrix} \phi_{rot} \\ \omega_{rot} \end{bmatrix}, \quad u_s = T_{1m,c}, \quad \mathbf{y}_s = \begin{bmatrix} \phi_{rot} \\ \omega_{rot} \end{bmatrix}, \quad (7a)$$

$$\mathbf{A}_s = \begin{bmatrix} 0 & 1 \\ 0 & 0 \end{bmatrix}, \quad \mathbf{B}_s = \begin{bmatrix} 0 \\ \frac{1}{J_{1m}} \end{bmatrix}, \quad x_d = F_r, \quad (7b)$$

$$\mathbf{E}_s = \begin{bmatrix} 0 \\ \frac{-1}{i_{APA} J_{1m}} \end{bmatrix}, \quad \mathbf{C}_s = \begin{bmatrix} 1 & 0 \\ 0 & 1 \end{bmatrix}. \quad (7c)$$

In the design of the disturbance observer, an auxiliary state that describes the unknown "dynamics" of the disturbance is added to the state vector. A simple autonomous system for constant disturbance is given by:

$$\dot{x}_d = A_d x_d, \quad y_d = C_d x_d, \quad (8a)$$

$$x_d = F_r, \quad A_d = 0, \quad C_d = 1, \quad (8b)$$

This is combined with Eq. (6) and leads to the extended system model

$$\begin{bmatrix} \dot{\mathbf{x}}_s \\ \dot{x}_d \end{bmatrix} = \begin{bmatrix} \mathbf{A}_s & \mathbf{E}_s C_d \\ 0 & A_d \end{bmatrix} \begin{bmatrix} \mathbf{x}_s \\ x_d \end{bmatrix} + \begin{bmatrix} \mathbf{B}_s \\ 0 \end{bmatrix} u_s, \quad (9a)$$

$$\mathbf{y} = \begin{bmatrix} \mathbf{C}_s & 0 \end{bmatrix} \begin{bmatrix} \mathbf{x}_s \\ x_d \end{bmatrix}. \quad (9b)$$

With a proper selection of the feedback gain matrix  $\mathbf{L}^T = [\mathbf{L}_1, \mathbf{L}_2]$ , and with the available measurements of the motor speed and position, the estimator (Luenberger observer) feedback term takes the form:

$$\mathbf{u}_e = \begin{bmatrix} \mathbf{L}_1 \\ \mathbf{L}_2 \end{bmatrix} (\mathbf{y} - \hat{\mathbf{y}}), \quad \hat{\mathbf{y}} = \begin{bmatrix} \mathbf{C}_s & 0 \end{bmatrix} \begin{bmatrix} \hat{\mathbf{x}}_s \\ \hat{x}_d \end{bmatrix} \quad (10)$$

and the disturbance observer state-space equation becomes:

$$\begin{bmatrix} \dot{\hat{\mathbf{x}}}_s \\ \dot{\hat{x}}_d \end{bmatrix} = \begin{bmatrix} \mathbf{A}_s - \mathbf{L}_1 \mathbf{C}_s & \mathbf{E}_s C_d \\ -\mathbf{L}_2 \mathbf{C}_s & A_d \end{bmatrix} \begin{bmatrix} \hat{\mathbf{x}}_s \\ \hat{x}_d \end{bmatrix} + \begin{bmatrix} \mathbf{B}_s \\ 0 \end{bmatrix} u_s + \begin{bmatrix} \mathbf{L}_1 \\ \mathbf{L}_2 \end{bmatrix} \mathbf{y}. \quad (11a)$$

A detailed derivation of this structure can be found in [26]. The observability of the extended system Eqn. (9) shows full rank using the Kalman observability criteria, so a full-state observer design is possible, including the unknown disturbance (rack force). The feedback gain matrix is calculated by the linear quadratic estimator (LQE) method which allows weighting the speed of convergence of the estimation error vs. the level of noise in the sensor measurements. For the test-rig evaluation of the proposed algorithm it is fundamental to synchronize the measurements of the speed and motor torque, which show a filter time delay in our test setup.

## RESULTS

### Friction Estimation Results

Fig. 9 shows the results of the estimation of the friction in a sine sweep dynamic maneuver. Here, the linear motor injects a sine sweep force signal with an amplitude of 750 Nm to the tie rods from 0 – 4 Hz. At the same time, the EPS motor simulates a spring-damper force to prevent the system from running in to its mechanical limits. To estimate the friction torque, the disturbance observer is re-configured and instead of the rack force (which is now available from a rack force sensor), the estimated disturbance is the friction. The plot compares the friction model output generated with the measured map (2Q-map, Fig. 4) and the one with the friction approximation (2Q-fa, Fig. 7). The zoomed view (upper right and lower left) show that excellent approximation is achieved in this maneuver. Note that at the beginning of the maneuver, where the rack force input is not high enough to overcome the friction and to move the system *and* when the EPS motor has zero torque, the estimated friction is not realistic. This is because of the speed-dependent friction model used in the FC module.

The parameters  $\sigma_0$ ,  $\sigma_{1,0}$  and  $\omega_{rot,\sigma_1}$  are set to the values listed in Tab. 2. The estimation showed minor sensitivity to variations of around these values during the sine sweep test procedure.

### Rack Force Estimation Results

Results for a simulation-based analysis of the rack force estimation algorithm are depicted in Fig. 10. Here, the same sine sweep input from the test-rig is injected in the simulation model of the EPS, and the EPS motor is controlled to act as a linear spring-damper force. It is obvious that the estimation without friction compensation (FC) shows large deviation from the rack force, while the friction approximation (here, considered to be the 2Q-fa) shows results close to the real rack force.

The performance of the rack force estimation scheme is also evaluated via the provisions of the test-rig and the physical EPS. Figure 11 shows the results for a sine sweep rack force input. The test shows promising results within the same performance

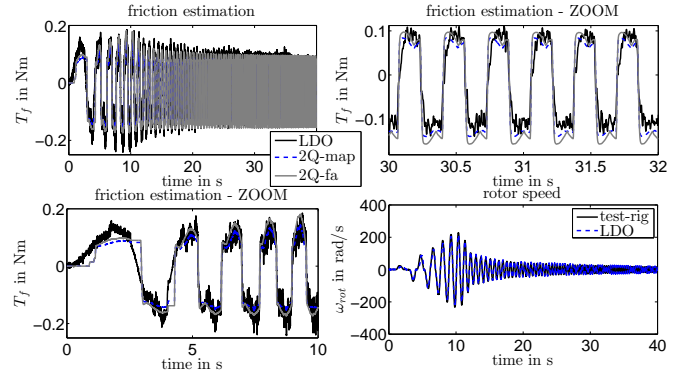


FIGURE 9. TEST RESULT FOR FRICTION ESTIMATION

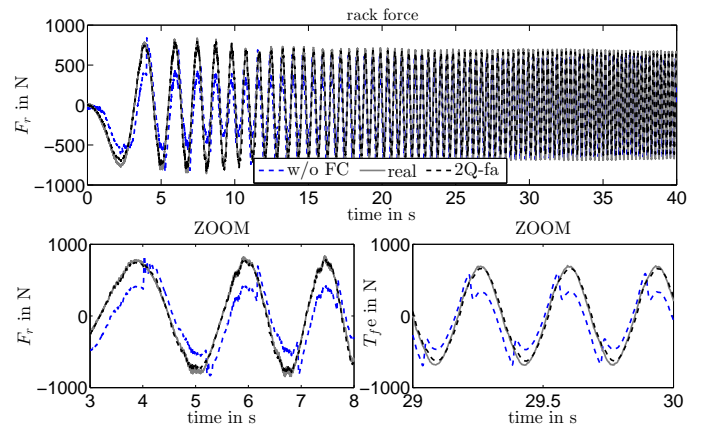
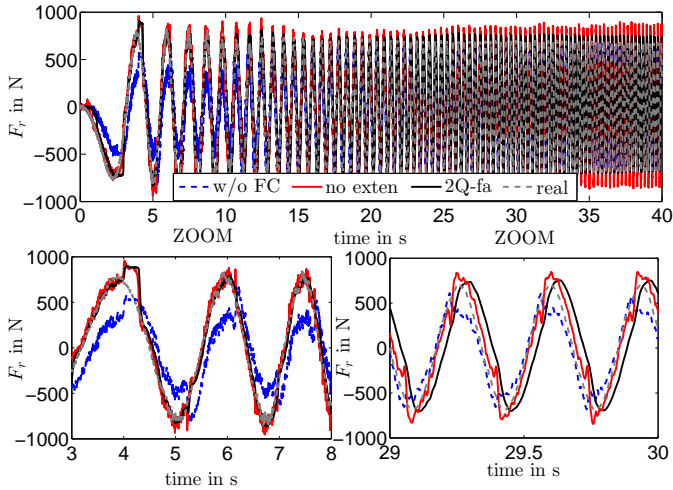


FIGURE 10. SIMULATION RESULTS FOR RACK FORCE ESTIMATION

range as in the simulation. At higher frequency, a small delay is seen which is caused by the low-pass filtering in the real system as depicted in Fig. 8. The low pass filtering is required to remove the noise of the sensors which is amplified by the observer. More important, the filter removes a peak seen in the estimation output in case of a non-correct parametrization of the synchronization module. In the given test, the result with label *no exten* shows mainly the effect from the filter as the other extensions are only active during small speed or stand-still conditions, see Eq. (4).

To show the effect of the additional limiting and dead-zone elements, the tests in Fig. 12 are included. Here, the rack force excitation is step-like. Again, the EPS motor is controlled to react as a spring-damper. Therefore, the system stops at a certain position after the rack force reaches a constant level and the speed is zero. The result shows that without the additional elements (label *no exten*) the rack force is not settling down on a constant value. This drift is caused by the noise in the speed sensor and in case of rack force-based steering feel generation, this could cause unwanted steering torque. The result with these ex-



**FIGURE 11.** TEST RESULT FOR RACK FORCE ESTIMATION USING THE TEST-RIG WITH RACK FORCE SWEEP EXCITATION

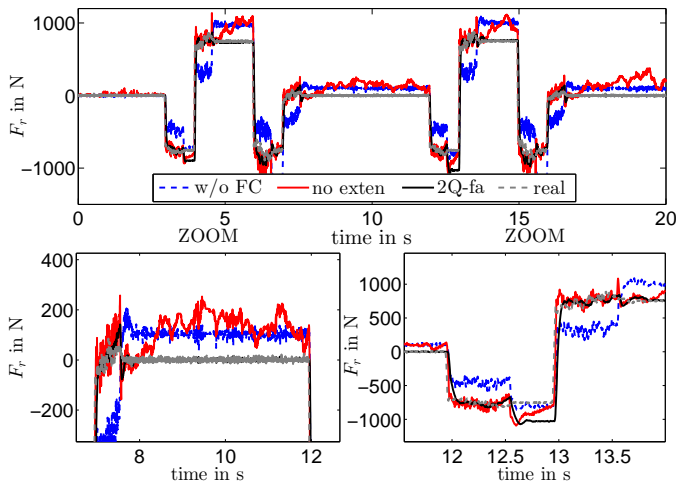


**FIGURE 12.** TEST RESULT FOR RACK FORCE ESTIMATION USING THE TEST-RIG WITH STEP-LIKE RACK FORCE EXCITATION

tensions shows the expected behavior of constant value in stand-still conditions and the estimation error is very small compared to no friction compensation. When the rack force and the EPS torque approach zero values, the friction compensation limiter reduces the compensation torque to zero, as otherwise a constant non-zero level is possible due to the hysteresis state  $z$  of the LuGre friction model, which depends on the history of speed.

## FRICION ADAPTATION

The results in the previous section assume that all the model parameters are known. In general, this is not the case, e.g. the friction varies during the lifetime of the steering device as a result of mechanical wear and also, each produced device shows a different level of friction due to manufacturing variations. Thus, the parameters identified above are only valid for the steering device on our test bench. Consequently, an adaptation of the friction parameters is necessary for an application in a real car.

Friction adaptation is a widely discussed topic. Overcompensation of Coulomb friction is seen critical in applications with PD position feedback-control with feedback friction compensation [27]. Suitable adaptation methods as presented in [18, 19] are useful to adjust the friction level and to prevent instability. However, stability is not critical in our applications, but the former proposed techniques use a control error to estimate the friction and system parameters and therefore, can not be used in the present application. Thus, the following alternative methods are suggested.

## Torque Injection

The first method to adapt the friction parameters is the injection of an artificial torque sequence with the EPS motor under predefined assumptions. The assumptions made here include a relatively small vehicle speed (e.g.  $v < 20$  m/s), straight driving (e.g. detected by small yaw rate and lateral acceleration  $< 0.05$   $m/s^2$ ), a low column sensor torque (e.g.  $T_{sen} < 1$  Nm), and the center position of the steering system. In this case, one can assume that the rack force is zero and the friction is the dominating disturbance. An important note is that only the friction offsets  $k_0^\pm$  are estimated assuming that the load- and speed-dependent values remain constant or are of minor significance. This is argued by the relatively small viscous damping found in the real system and the fact that the relation of normal load between mechanical elements and friction is linear. Observations from real steering systems show that in the on-center position, a small dead-zone is found before the tire aligning force acts on the tie rods, e.g. a backlash in all mechanical parts between rack and tire. Thus, when the driver turns the steering wheel, first the pinion starts rotating, then a rack movement is detected and then the ball gear and the rotor start to rotate. Finally, the wheels start turning around the steering axis. The torque injection uses this fact to move the rack until a change in driver torque or a predefined speed set-point is reached. Figure 14 shows the adaptation flag and the direction in which it is adapted (upper left plot), while the lower right curves show the injected torque and the column sensor torque. In this test, the driver is in hands-on mode and counteracts the injected torque after the friction torque is compensated and the rack starts moving (lower left plot). Then, the ramp-type injected torque is set to zero and the last value is set as the new value for the friction offset  $k_0^\pm$ .

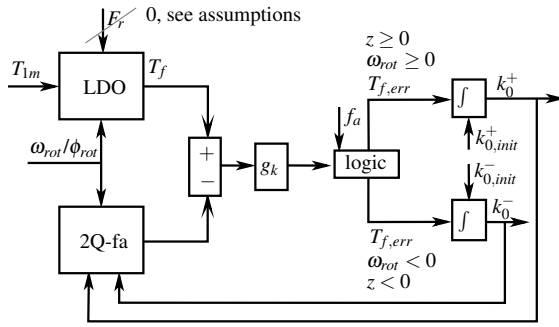


**FIGURE 13.** OVERVIEW ABOUT FRICTION PARAMETER ADAPTION WITH ERROR INJECTION

### Error Injection

In contrast to torque injection, error injection does not necessarily require an active input from the EPS motor. Instead, the same prerequisites are used here, but the input from the driver serves together with the EPS motor as input. The driver applies torque to the steering wheel as long as no hands-off situation is found. Thus, the steering device is excited and small speed is measured if the driver torque is of sufficiently high value. A fusion of all conditions to a single adaptation-flag as in the torque injection method enables the adaptation. Then, the output of the friction model is compared to the torque input to the steering system. The error is multiplied by an adaptation gain  $g_k$  and then forwarded to a speed direction sensitive integrator for each direction, see Fig. 13. The selection of the parameter to adapt is done by both the sign of the speed measurement and the sign of the friction model state  $z$ . Only when both signs are equal is the adaptation enabled. This is important as small movements of the steering rack are used for the adaptation where hysteresis plays an important role.

To compare the results of both injection approaches, the schemes are activated during the same test using the numerical simulation. The result in the upper right subplot of Fig. 14 shows that error injection gives slightly better results, but in general both algorithms are suitable to estimate the asymmetric offset under the given assumptions. To loosen the assumptions, other techniques such as unscented Kalman filtering (UKF) were analyzed including the nonlinear friction and the steering system dynamics, but no convergence was found. In anywise, the computational burden there is clearly higher than for the above injection-type methods.

### CONCLUSION

Modern steering systems with electric motors enable several new driver assistance functions due to their excellent control behavior. The main goal of the work was to find a simple algorithm with low computational burden for the estimation of the steer-

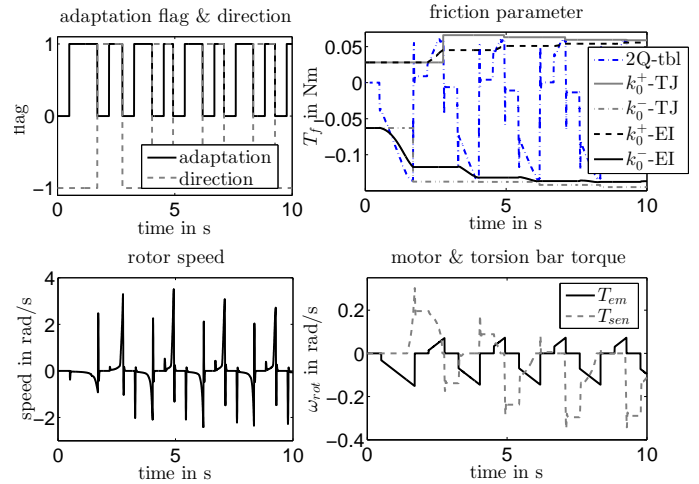


**FIGURE 14.** FRICTION PARAMETER ADAPTATION: COMPARISON OF TORQUE INJECTION (TI) VS. ERROR INJECTION (EI)

ing rack force that could be used to further improve and expand the functionality of modern EPS. To this end, a modern electric power steering device was modeled and analyzed by measurements on a high fidelity steering test-rig. In particular, the LuGre friction model was adopted and modified by introducing the experimentally identified characteristics of the load (rack force) and speed-dependent friction in the steering application. There in, no Stribeck effect was found which reduced the numbers of parameters of the friction model. The identified two-dimensional static friction map part of the model was then approximated by a linear function of the steering speed and the rack force. The friction model was then combined with a linear disturbance observer to estimate the rack force as an unknown disturbance. It was observed that at lower rack force levels, the friction compensation is shown to be of particular importance. The results from the test-rig with the proposed rack force estimator depicted the high accuracy as long as all model parameters are known. The contribution ends with suggestions for some adaptation schemes to account for potentially unknown friction model parameters on a real vehicle.

### REFERENCES

- [1] Fankem, S., and Müller, S., 2014. "Steering feel generation in steer-by-wire vehicles - modular steering torque computation and requirements for the hand wheel actuator". In Proceedings of the 5th International Munich Chassis Symposium.
- [2] Dannöhl, C., Müller, S., and Ulbrich, H., 2012. " $h_\infty$ -control of a rack-assisted electric power steering system.". *Vehicle System Dynamics*, 50(4), pp. 527–544.

- [3] Hsu, J., 2009. “Estimation and control of lateral tire forces using steering torque”. PhD thesis, Stanford University.
- [4] Weiskircher, T., and Müller, S., 2012. “Nonlinear state estimation of vehicle dynamics for a road vehicle with independent rim-mounted electric drives”. In 11th International Symposium on Advanced Vehicle Control.
- [5] Koch, T., 2009. “Assessment of steering feel in a sports car equipped with a steer-by-wire system”. In Aachener Kolloquium Fahrzeug- und Motorentchnik, pp. 594–508.
- [6] Nehaoua, L., Djemai, M., and Pudlo, P., 2012. “Rack force feedback for an electrical power steering simulator”. In 20th Mediterranean Conference on Control & Automation (MED), pp. 79–84.
- [7] Fankem, S., Weiskircher, T., and Müller, S., 2014. “Model-based rack force estimation for electric power steering”. In Proceedings of the 19th IFAC World Congress.
- [8] Armstrong-Helouvry, B. “Dynamic friction in the control of robots”. In IEEE International Conference on Robotics and Automation, Vol. 2, pp. 1202 – 1207.
- [9] Armstrong-Helouvry, B., Dupont, P., and de Wit, C. C., 1998. “Friction model and friction compensation”. *European Control Journal*(4), pp. 176–195.
- [10] Olsson, H., Astrom, K., de Wit, C. C., Graefvert, M., and Lischinsky, P., 1998. “Friction models and friction compensation”. *European Journal of Control*, **4**(3), pp. 176–195.
- [11] Astrom, K., and de Wit, C. C., 2008. “Revisiting the lugre model”. *IEEE Control Systems Magazine*, **28**(6), pp. 101–114.
- [12] Futami, S., Furutani, A., and Yoshida, S., 1990. “Nanometer positioning and its micro-dynamics”. *Nanotechnology*, **1**(1).
- [13] Panteley, E., Ortega, R., and Gaefvert, M., 1998. “An adaptive friction compensator for global tracking in robot manipulators”. *Systems & Control Letters*, **33**, pp. 307–313.
- [14] Ray, L., Ramasubramanian, A., and Townsend, J., 2001. “Adaptive friction compensation using extended kalman-bucy filter friction estimation”. *Control Engineering Practice*, **9**, pp. 169–179.
- [15] Tjahjowidodo, T., Al-Bender, F., Brussel, H. V., and Symens, W., 2007. “Friction characterization and compensation in electro-mechanical systems”. *Journal of Sound and Vibration*, **308**, pp. 632–646.
- [16] Yazdizadeh, A., Noorbakhsh, S., and Barzamini, R., 2009. “A new lyapunow-based design scheme for adaptive friction compensation”. *Journal of Applied Sciences*, **9**(9), pp. 1668–1676.
- [17] Xu, Q., and Li, Y., 2010. “Dahl model-based hysteresis compensation and precise positioning control of an xy parallel micromanipulator with piezoelectric actuation”. *Journal of Dynamic Systems, Measurement, and Control*, **132**, pp. 1–12.
- [18] Xie, W.-F., 2007. “Sliding-mode-observer-based adaptive control for servo actuator with friction”. *IEEE Transactions on Industrial Electronics*, **54**(3), pp. 1517–1527.
- [19] Ahmed, F. S., Laghrouche, S., and Bagdouri, M. E., 2012. “Cascaded second order sliding mode observer for state and friction dynamics of a control valve”. In 12th IEEE Workshop on Variable Structure Systems.
- [20] Stauder, S., Müller, S., Plöger, A., and Lehmann, A., 2012. “Concept of a new hardware-in-the-loop driving simulator for the model-based design of mechatronic steering systems”. In 12th Stuttgart International Symposium, Automotive and Engine Technology.
- [21] Nouri, B. M. Y., 2004. “Friction identification in mechatronic systems”. *ISA Transactions*(43), pp. 205–216.
- [22] Kim, M., and Chung, S., 2006. “Friction identification of ball-screw driven servomechanisms through the limit cycle analysis”. *Mechatronics*, **16**, pp. 131–140.
- [23] Rizos, D., and Fassiois, S., 2009. “Friction identification based upon the lugre and maxwell slip models”. *Transactions on Control Systems Technology*, **17**(1), pp. 153–160.
- [24] Hamon, P., Gautier, M., Garrec, P., and Janot, A., 2010. “Dynamic identification of robot with a load-dependent joint friction model”. In IEEE Conference on Robotics Automation and Mechatronics (RAM), pp. 129 – 135.
- [25] Marton, L., Fodor, S., and Sepehri, N., 2011. “A practical method for friction identification in hydraulic actuators”. *Mechatronics*, **21**, pp. 350–356.
- [26] Franklin, G. F., Powell, J. D., and Emami-Naeini, A., 2006. *Feedback control of dynamic systems*. Prentice Hall, Princeton, N.J.
- [27] Putra, D., and van de Wouw, H. N. N., 2007. “Analysis of undercompensation and overcompensation of friction in 1dof mechanical systems”. *Automatica*, **43**, pp. 1387–1394.